Breast Disease 25 (2006) 43–69
IOS Press

Poster Presentations – Sunday, September 17

SP1
DOCK4 IS FREQUENTLY EXTINGUISHED IN SPORADIC BREAST CANCER

Aghajani A.[1], Balkhi S.[1], Sirati F.[2], Najmabadi H.[1] and Ohadi M.[1]
[1]*University of Social Welfare and Rehabilitation, Tehran, Iran;* [2]*Mehrad Hospital, Tehran, Iran*

Loss of heterozygosity at 7q31 is among the most frequent genetic abnormalities associated with sporadic breast cancer. The tumor suppressor gene, dedicator of cytokinesis 4 (DOCK4), is involved in the induction of adherens junctions resides at this locus. The aim of this study was to analyze the expression of this gene in a panel of normal (n= 18), and sporadic breast cancer tumor specimens (n=34), and compare its expression with parameters of grade and stage of the disease. DOCK4 mRNA was detected in 15/18 (83%) of normal specimens and 16/34 (47%) of the breast tumor specimens (c2= 6.43, $p<0.025$). No correlation was observed between the stage of the tumor and expression of the DOCK4 gene ($P < 0.3$). For the first time, these findings implicate that DOCK4 is frequently extinguished in the course of tumorigenesis of breast cancer. This may explain a mechanism of evasion from contact inhibition in this type of cancer.

SP2
IMAGING OF TUMOR-TARGETING QUANTUM DOT IN BREAST CANCER OF LIVING MICE

Tada H.[1], Higuchi H.[2], Watanabe T.[2] and Ohuchi N.[2]
[1]*Tohoku University, Sendai-shi, Miyagi, Japan;*
[2]*Tohoku University, Sendai, Japan*

Recent anti-cancer therapeutics has been based on an active tumor targeting by conjugating antibodies against tumor-associated antigens such as HER2, for increasing therapeutic efficacy and decreasing systemic toxicity. However, the specific processes of the antibody delivery in vivo post injection are not known at the molecular level. Here we report the imaging of fluorescent nanoparticle conjugated with anti-HER2 antibody in living mice using a high speed confocal microscope. Semiconductor quantum dot (Qdot) are nanometer-sized crystals which improved brightness, resistance against photobleaching compared with organic dyes and fluorescent proteins. After intravenous injection of the tumor targeting quantum dot to living mouse with breast cancer, the accumulation of QDs to the tumor tissue was clearly observed at subcellular resolution with the original 3D intravital microscopic system. And we successfully track the movement of single particle of tumor targeting quantum dot in living mouse tumor tissue. This suggests that we can eventually develop a novel cancer imaging and drug tracking system. The tracking method used in our experiments is a powerful tool for developing drug delivery system to know where is a bottleneck in complex tumor microenvironments.

SP3
METACHRONOUS BILATERAL BREAST CANCER DISTINGUISHES BRCA1/2-POSITIVE FROM MUTATION-NEGATIVE FRENCH CANADIAN BREAST/OVARIAN CANCER FAMILIES

Tonin P.[1] and the Montreal Hereditary Breast-Ovarian Cancer Study Group
Research Institute of the McGill University Health Centre, Montreal, QC, Canada

Our group has shown that ~ 40% of French Canadian breast/breast-ovarian cancer families harbor germline BRCA1/2 mutations, where >80% are 1 of 5 recurrent mutations. Various mutation prediction programs were applied to a well characterized series of French Canadian cancer families (N=224) comprised of at least 3 cases of breast (Dx <65 yrs) and/or ovarian cancer occurring in 1st- , 2nd-, and/or 3rd-degree relatives of affected index case with known carrier status: 44 BRCA1-postive and 52 BRCA2-positive families, and 128

3956 breast and/or ovarian, prostate, colorectal and male breast cancer cases and 3591 controls.
Results: The frequency of Cys557Ser appeared to be increased among familial breast and/or ovarian cancer cases, when compared to healthy controls (p=0.001).
Conclusion: Our results provide further evidence that *BARD1* Cys557Ser confers a slightly increased risk of breast cancer.

SP10
DETECTION OF SENTINEL LYMPH NODES BY NOVEL MR CONTRAST MEDIA

Takeda M.[1], Kobayashi Y.[2], Sakurai Y.[3], Cong L.[3], Ishida T.[3], Suzuki A.[3], Amari M.[3] and Ohuchi N.[3]
[1]Graduate School of Engineering, Tohoku University, Sendai, Japan; [2]Ibaraki University, Hitachi, Japan; [3]Graduate School of Medicine, Tohoku University, Sendai, Japan

Sentinel lymph node (SN) navigation surgery has been widely accepted as a method for made-to-order and low-invasive medicine. The size of particles is the most important factor for SN detection. We previously decided the suitable size for SN detection as 40nm by animal experiments. In this study, we aimed to clarify possibility of nano-sized particles of MR contrast media with appropriate size to make up disadvantages of existing methods like radioisotope or dye methods.
We developed nano-sized gadolinium beads in size of 40-60nm. We took MR imaging of the suspension of gadolinium nano-particles. And we injected the suspension of gadolinium beads into the rat's foot pad of the hind leg subcutaneously and followed MR scanning of the inguinal area for SN detection.
The nano-sized gadolinium beads exhibited higher signal intensity than water. It also showed changes of signal intensity in inguinal lymph nodes.
Existing contrast media for MRI passes so fast through lymph nodes that the timing of administration is difficult. As appropriate sizes allow nano-particles to stay at lymph nodes for a while, we could detect gadolinium nano-particles before and during surgery like radioisotopes. In conclusion, we claim that the nano-sized gadolinium beads have a potential to be an alternative to existing tracers for SN detection.

SP11
APPLICATION OF NANOTECHNOLOGY FOR BREAST CANCER RESEARCH: NANO-DDS AND MOLECULAR IMAGING BASED ON VISUALIZATION OF SINGLE PARTICLE IN VIVO

Ohuchi N.[1], Takeda M.[2], Nakajima M.[1], Sakurai Y.[1], Kawai M.[1], Ishida T.[1] and Higuchi H.[3]
[1]Graduate School of Medicine, Tohoku University, Sendai, Japan; [2]Graduate School of Engineering, Tohoku University, Sendai, Japan; [3]Biomedical Engineering Research Organization, Tohoku University, Sendai, Japan

Nanomedicine is the application of nanotechnology to prevention, diagnosis and treatment of human disease. It has a potential to change medical science dramatically in the 21st century. However, the research field is in its infancy, and it is necessary to grasp mechanism of pharmacokinetics, the toxicity on the occasion of application to medical treatment, in particular on the aspect of safety of the materials and devices. Here, we describe fluorescent nono-particles for sentinel node navigation for breast cancer surgery in experimental model, which have shown the potential to be an alternative to existing tracers in the detection of the sentinel node of if we select the appropriate particle size and wavelength. We also describe generation of CdSe nanoparticles, Quantum Dots (QDs) conjugated with monoclonal anti-HER2 antibody, Trastuzumab, for molecular imaging of breast cancer cells. The QDs-Trastuzumab complex coated with PEG was successfully made without decreasing the titer of antibody. We established a high resolution of 3D in vivo microscopic system as a novel imaging method at molecular level. The cancer cells expressing HER2 protein were visualized by the nanoparticles in vivo at subcellular resolution, suggesting future utilization of the system in medical applications including drug delivery system to target the primary and metastatic tumors. Future innovation in cancer imaging, not only at cellular level but also at molecular level, by synthesizing diagnostic agents with nanoparticles, is now expected.

Overlapping hand-over-hand mechanism of single molecular motility of cytoplasmic dynein

Shiori Toba*†, Tomonobu M. Watanabe‡, Lisa Yamaguchi-Okimoto*, Yoko Yano Toyoshima*, and Hideo Higuchi‡§

*Department of Life Sciences, Graduate School of Arts and Sciences, University of Tokyo, 3-8-1 Komaba, Meguro-ku, Tokyo 153-8902, Japan; and ‡Biomedical and Engineering Research Organization, Engineering Research Laboratory Complex 901, Tohoku University, 6-6-11 Aramaki, Sendai 980-8579, Japan

Edited by James A. Spudich, Stanford University School of Medicine, Stanford, CA, and approved February 11, 2006 (received for review September 29, 2005)

Structural differences between dynein and kinesin suggest a unique molecular mechanism of dynein motility. Measuring the mechanical properties of a single molecule of dynein is crucial for revealing the mechanisms underlying its movement. We measured the step size and force produced by single molecules of active cytoplasmic dynein by using an optical trap and fluorescence imaging with a high temporal resolution. The velocity of dynein movement, 800 nm/s, is consistent with that reported in cells. The maximum force of 7–8 pN was independent of the ATP concentration and similar to that of kinesin. Dynein exhibited forward and occasional backwards steps of ≈8 nm, independent of load. It is suggested that the large dynein heads take 16-nm steps by using an overlapping hand-over-hand mechanism.

microtubules | motor protein | optical tweezers | step size | nanotechnology

Dynein is a molecular motor that moves along microtubules to the direction of the minus end. Cytoplasmic dynein transports cellular organelles toward the minus end of microtubules, whereas most kinesin molecules transport organelles toward the plus end (1–3). Hirakawa *et al.* (4) have reported that purified axonemal dynein produced maximum forces of 5 pN, and they also showed stepwise displacements of 8 nm. In contrast, another study (5) has demonstrated that single molecules of purified cytoplasmic dynein move with short steps (8 nm) at high loads (>0.8 pN) and long steps (16–32 nm) at low forces (<0.4 pN), and from these findings a molecular gear mechanism was proposed. The values for maximum force and the size of the steps differ between those two reports. Moreover, the very low velocity (<50 nm/s) of movement of the purified cytoplasmic dynein (5) is in direct contrast to the high velocity (≈1 μm/s) of dynein movement in a cell and in an *in vitro* motility assay (6–8). These discrepancies possibly result from inactive dynein molecules being included with the purified native dynein in the analysis.

In this study a method of coating the beads with dynein was developed to keep dynein active and allow the force and step size produced by single molecules of dynein to be measured. The step size of active cytoplasmic dynein was 8 nm and was independent of both force and ATP concentration. The stall force was 7–8 pN. These values are very similar to those recorded for kinesin (9); however, the stepping manner was different from that of kinesin.

Results

Active Dynein Bound to Protein A-Coated Beads. The method used to purify cytoplasmic dynein without its accessory protein, dynactin, has been described (Fig. 1*a*, lane D) (10, 11). Dynein was further purified by allowing it to bind to the microtubules (Fig. 1*a*, lane AMP-PNP) (12). Dynein was then released from microtubules in the presence of 0.1–10 mM ATP (Fig. 1*a*, lane ATP).

The method used to bind dynein to the coverslips for *in vitro* motility assay and beads for optical trap assay was modified from previously reported methods (5, 8). Beads coated with protein A were suitable for motility and force generation. With dynein attached to glass coverslips and bound to microtubules marked at the minus end, the microtubules moved with the marked end trailing. This result indicated that dynein moved toward the minus end of the microtubule. Polystyrene beads, 0.2 μm in

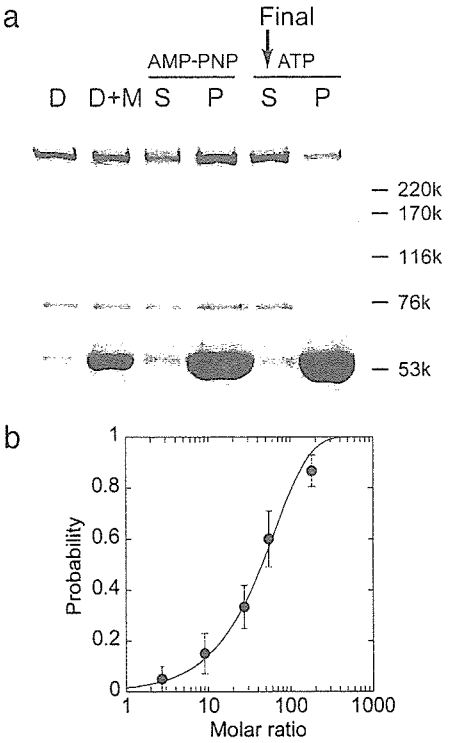

Fig. 1. Purification and force generation of single cytoplasmic dynein molecules. (*a*) SDS/PAGE of dynein purification. D lane, dynein purified by the anion-exchange column. D+M lane, dynein mixed with the microtubules. S and P indicate supernatant and pellet, respectively, after dynein mixed with the microtubules was centrifuged in the presence of 0.1 mM adenosine 5′-[β,γ-imido]triphosphate (AMP-PNP). After the pellet was suspended, it was centrifuged in the presence of 10 mM ATP. The supernatant was then used for the experiment. Numbers on the right indicate molecular mass in kDa. (*b*) The probability of the moving beads relative to the total beads was calculated. The molar ratio is the ratio of the bead concentration to the dynein concentration (10–20 nM) at the time of mixing. The probability was fitted to the curve, $1 - \exp(-x/65)$, indicating that single molecules produced the force.

Conflict of interest statement: No conflicts declared.

This paper was submitted directly (Track II) to the PNAS office.

Freely available online through the PNAS open access option.

†Present address: Kansai Advanced Research Center, National Institute of Information and Communications Technology, Kobe, Hyogo 651-2492, Japan.

§To whom correspondence should be addressed. E-mail: higuchi@tubero.tohoku.ac.jp.

diameter, were coated with protein A. Freshly purified dynein was bound to the beads coated with protein A. Beads were trapped and brought into contact with the microtubule. Displacement and force were measured with very high temporal resolution by using small beads (9). Experiments were performed within 2 h after protein purification to ensure that active dynein was used in the measurements.

The fraction of beads that moved processively increased exponentially with the increase in the ratio of dynein to the beads, indicating that single molecules of dynein move processively (Fig. 1*b*) (4, 13, 14). The fraction of beads that bound to microtubules in the presence of 1 mM adenosine 5′-[β,γ-imido]triphosphate (AMP-PNP) was almost the same as the fraction that moved in the presence of 1 mM ATP. Dynein binds tightly to microtubule in the presence of AMP-PNP (12). This finding also provides support for the conclusion that single molecules move processively (4). The ratio of beads-to-dynein molecules required to move 50% of the beads was ≈40:1, which was considerably lower than the value obtained by using dynein on a noncoated bead (5) (Fig. 5, which is published as supporting information on the PNAS web site). The ratio was also lower than the value (>120:1) when the beads were coated with BSA or casein. This result indicates that beads coated with protein A provide a suitable medium for dynein to bind. Experiments measuring step size and force were performed at a ratio of 0.1:0.3 of the mobile-to-immobile beads, where >95% of the beads that moved and produced force were caused by single molecules of dynein (9).

Force–Velocity Relation of Single Dynein Molecules. Single molecules of dynein moved processively and produced forces up to 7–8 pN in the presence of 1 mM ATP (Fig. 2*a*). The dynein bound to beads coated with BSA or casein also produced forces of ≈7 pN, indicating that protein A coating did not modify the motility of dynein. However, when the beads were not coated with the proteins low forces and velocities were often observed similar to those reported in a previous study (5) (Fig. 5). This result suggests that the presence of protein A is important for keeping dynein active.

To confirm the direction of movement, beads with dynein attached were mixed with kinesin-1 molecules. Directional movement in both the forward and backward directions was observed, confirming that the direction of movement by single molecules of dynein is opposite to that of kinesin (Fig. 2*b*).

The force trace of dynein movement is very similar to that of kinesin other than the direction (Fig. 2*b*). To confirm the similarity, the relationship of force to velocity was obtained by analysis of 20–30 traces (Fig. 2*c*). The velocity of dynein decreased with increased force. The velocity at low forces and high ATP concentrations of ≈800 nm/s is consistent with that observed in cells and *in vitro* assays (0.5–1.5 μm/s) (6–8). At low ATP concentrations (10 μM), the velocity decreased and the stall force of ≈7 pN was independent of the concentration of ATP (Fig. 2*c*). The velocity at low forces is about half that obtained for kinesin-1 [Fig. 2*c*, dashed blue line (9)]. This distinction explains the difference in K_m values, i.e., ATP concentration at the half-maximal activated ATPase activity between kinesin-1 and dynein. The K_m value of cytoplasmic dynein was measured to be 89 μM, which is 2.5-fold larger than that of kinesin-1 [36 μM (9)].

Step Size of Single Dynein Molecules. Single molecules of cytoplasmic dynein moved stepwise at ATP concentrations of 1 mM and 10 μM (Fig. 3 *a* and *c*). Steps of 8 nm were clearly detected in the expanded traces (Fig. 3 *a* and *c* Insets). Steps of 8 nm were also observed at very low forces of <0.3 pN as measured with a trap laser at low power (Fig. 3*e*). Backward 8-nm steps were also occasionally detected (Fig. 3 *c* and *e*).

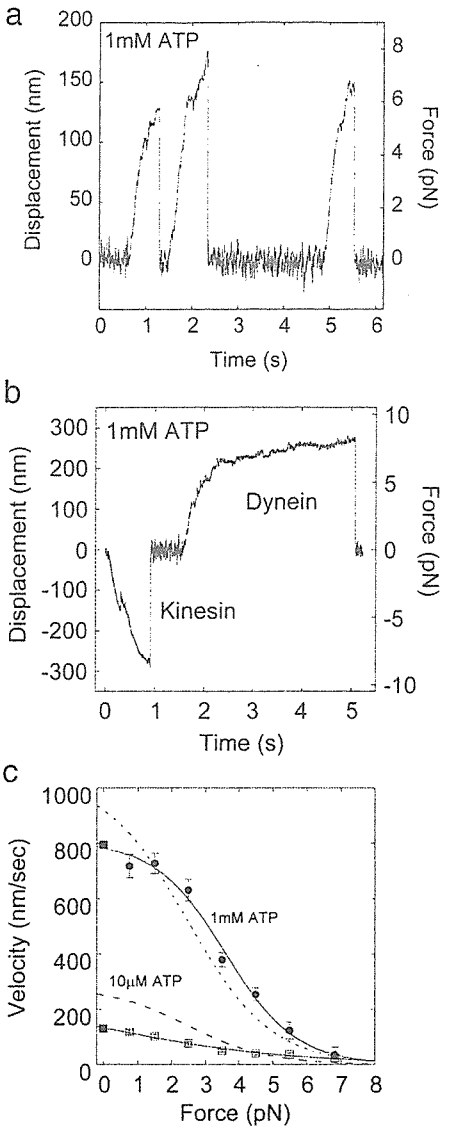

Fig. 2. Force generation by single cytoplasmic dynein molecules. (*a*) Bead movement in the presence of 1 mM ATP at a trap stiffness of 45 fN/nm. Force reached 6–8 pN before the dynein molecule dissociated from the microtubule. (*b*) Dynein beads were mixed with kinesin at a ratio of 10:1 in the presence of 1 mM ATP at a trap stiffness of 30 fN/nm. (*c*) Force–velocity dependence at 1 mM (red circles) and 10 μM ATP (violet squares). Velocity was calculated from the displacement (20–30 nm) divided by the time taken to cover this distance. Each symbol is the average value of the velocities from 20–30 individual force traces. Velocities at zero force were measured by using an *in vitro* motility assay (closed squares). Dotted line indicates the force–velocity relation of bovine kinesin-1 from a previous study (9).

Step sizes of >4 nm were analyzed over the range of 1 to 7 pN. A major peak was observed at ≈8 nm and minor peaks were seen at 16 and −8 nm (Fig. 3 *b* and *d*). The 16-nm steps were assumed to be rapid double steps of 8 nm generated with a temporal resolution of 4 ms or less. The observed step size was ≈8 nm and was independent of force in the range of 1–7 pN and the ATP concentration.

A previous study by Mallik *et al.* (5) found that the step size of single dynein molecules increased to 16–24 nm at low (<0.8 pN) or zero force. Here, the step size at low forces of <1 pN was measured at a low laser trap stiffness (Fig. 3*e*). A histogram of step size at forces in the range 0.0 to 0.9 pN indicated a major peak at 8 nm (Fig. 3*f*). The step size at low forces was 8–9 nm and was independent of force.

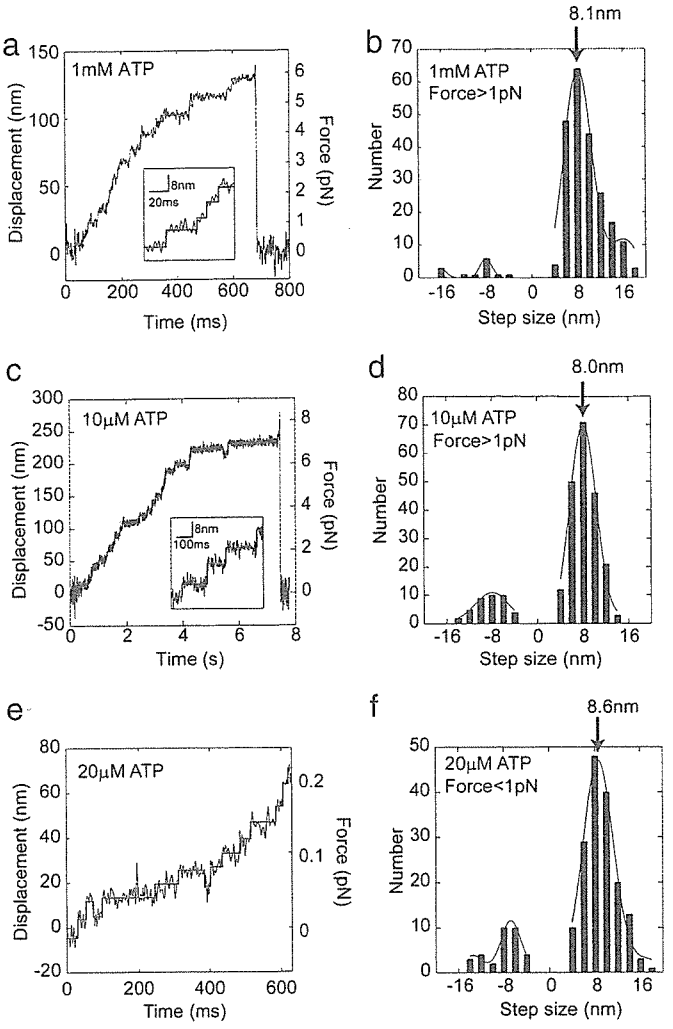

Fig. 3. Step size of single dynein molecules. (*a* and *c*) Stepwise movement at high concentration (1 mM, *a*), and low concentration (10 μM, *c*) of ATP. (*a and c Insets*) Expanded traces of the stepwise movement. (*e*) Bead movement in 20 μM ATP at a trap stiffness of 3.0 fN/nm. (*a*, *c*, and *e*) Step sizes of >4 nm and dwell times of >5 ms (*a*) and >20 ms (*c* and *e*) were fitted to a rectangular curve (30) (blue line). (*b*, *d*, and *f*) Histograms of step sizes. (*b*) ATP concentration of 1 mM and forces >1 pN. (*d*) ATP concentration of 10 μM and forces >1 pN. (*f*) ATP concentration of 20 μM and forces <1 pN. The histograms *a*–*c* were fitted to a Gaussian curve with the center at a multiple of the unit step size of 8.1, 8.0, and 8.6 nm, respectively.

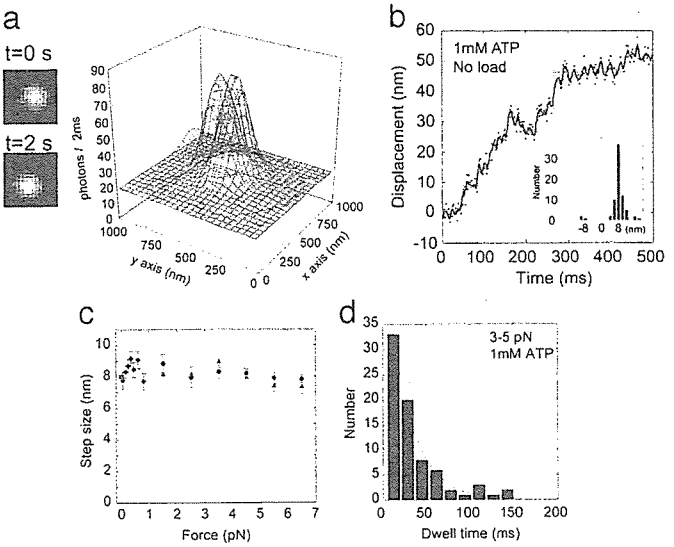

Fig. 4. Step sizes and dwell times. (*a*) Fluorescence images and profiles of the images of a quantum dot dynein interacting with a microtubule. The green-colored profile was taken at time 0 and the red profile was taken at $t = 2$ s. (*b*) Displacements of single dynein molecules at 2-ms intervals were determined by the intensity profiles fitted to 2D Gaussian curves (red dots). Three points were averaged to reduce noise (black line). Step sizes were automatically detected by using computer programming (blue line). (*Inset*) A histogram of the step size with a peak at 8.0 nm. (*c*) Step sizes were measured at high trap stiffness and ATP concentrations of 1 mM (circles) and 10 μM (triangles). Step sizes at low trap stiffness and 20 μM ATP (diamonds) and zero load (squares) were obtained. The average step size was 8.1 nm. (*d*) Dwell time between adjacent steps. The time was measured at 3- to 5-pN force in the presence of 1 mM ATP. The dwell time was fitted to a single exponential curve to obtain a time constant of 27 ms.

The movement of single dynein molecules was measured at zero load without a laser trap by using fluorescence imaging with 1-nm accuracy (15). The intensity of organic fluorescence dyes such as Cy3 is too weak to be used for measurements at high temporal resolutions <100 ms (15). The step dwell time of cytoplasmic dynein was ≈10 ms. To improve the temporal resolution and lifetime of the fluorescence, dynein was bound to CdSe quantum dots, which are very stable and have an intense fluorescence (16). To slow the movement of dynein, the temperature was decreased to 16°C. At an exposure time of 2 ms, clear images were obtained (Fig. 4*a* and Fig. 6, which is published as supporting information on the PNAS web site). The position of dynein was determined by fitting a profile of the fluorescence intensity to a 2D Gaussian curve (Fig. 4*a*). These methods showed that the step size of dynein is 8 nm (Fig. 4*b*). The histogram of step sizes showed a major peak of 8.0 nm and a minor peak at 16 nm (Fig. 4*b Inset*).

The step sizes at various forces and ATP concentrations are summarized in Fig. 4*c*. The step size of 8 nm was independent of force over the range 0 to 7 pN and ATP concentration over the range 10 μM to 1 mM. The average of all of the data was 8.1 nm.

The time taken from the beginning of one step to the beginning of the next step was analyzed as the dwell time and was used to determine the step reaction rate and the number of rate-limiting steps. The histogram of the dwell time at forces of 3–5 pN showed an exponential decay with a time constant of 27 ms (Fig. 4*d*), indicating that a rate-limiting state is one with a rate of 37 per s.

Discussion

The stall force of single molecules of cytoplasmic dynein in the laser trap assays was 7–8 pN and was independent of the ATP concentration and load. The stall force and step size of cytoplasmic dynein were consistent with the results for axonemal dynein [≈6 pN (17); ≈5 pN and 8 nm (4)] and cytoplasmic dynein in a cell (8 nm) (18). However, these results are inconsistent with previous findings of low force, low velocity, and a long step size for cytoplasmic dynein (5). These discrepancies are most likely caused by the active state of dynein. Improvements of the bead-coating method and temporal resolution of the optical trap made it possible to measure the fast movement of the active dynein molecules. This idea is supported by the fact that the low forces and velocity are similar to those in a previous study (5) when the bead was not coated (Fig. 5).

The single exponential decay of the dwell time distribution indicates only one rate-limiting state in an 8-nm step (14). Maximum ATPase rate and the sliding velocity of recombinant single-headed dynein was 160 per s and 1,200 nm per s, respectively (12). From these values, the sliding distance of single-headed dynein was calculated to be 7.5 nm per ATP molecule

hydrolyzed. These results suggest that 8-nm steps of single molecules of dynein are coupled with the hydrolysis of ATP molecules under our experimental conditions. Dynein has four potential ATP binding and hydrolysis sites, and one site, P1, is the primary site for ATPase activity (19). Thus, 8-nm steps would be coupled with ATP hydrolysis mainly in the P1 site.

The maximum velocity, stall force, and step size of the cytoplasmic dynein are strikingly similar to those reported for kinesin-1 (9, 13, 14, 20). Hand-over-hand and inchworm models for kinesin have been proposed previously (14, 21–24). The hand-over-hand mechanism was supported by the results that kinesin-1 has an asymmetrical dwell time and the head takes 16-nm steps (21–23). The result that dynein has one rate-limiting state at the 8-nm step supports the hand-over-hand model because the simple inchworm model requires two step reactions to produce one 8-nm step (21, 22). Therefore, each dynein head steps by 16 nm, whereas dynein molecule steps by 8 nm.

The dynein head differs greatly from kinesin-1 in structure, size, and amino acid sequence. The diameter of the ring-shaped dynein head is 15 nm, which is almost 2-fold greater than the step size. How then does dynein step by 8 nm with a hand-over-hand mechanism? Electron microscopy of dynein shows a Φ-shaped structure, indicating that the tails of the two heads are close to each other and the ring domains partially overlap (10, 25). When the heads of dynein bind to the microtubule, they also overlap (25–27). A possible model to explain the stepping movement is that the dynein heads are positioned axially along the microtubule similar to kinesin. Thus, the ring regions representing the dynein heads should overlap.

Force generation can be explained by structural changes between dynein head and tail that are predicted to occur at the different chemical states; one state is at the power stroke and the other at the recovery stroke (28, 29). Other than specific structural changes, the similarity of the mechanical properties of dynein, e.g., backward steps, step size, and stall force, to those of kinesin-1 predicts that Brownian motion and possibly biased binding of the heads are essential components in the molecular mechanism underlying the dynein steps (9, 20, 30).

Materials and Methods

Preparation of Dynein and Kinesin. Cytoplasmic dynein and kinesin-1 were purified from porcine brain as described (9–11). Purified dynein in 25% sucrose was rapidly frozen and stored in liquid nitrogen. Just before an experiment, dynein was further affinity-purified by binding to the microtubules (12). Microtubules used in motility assays, and laser trap measurements were prepared from tubulin purified from porcine brains and labeled with tetramethylrhodamine.

Laser Trap Measurements. Polystyrene beads of 0.2 μm in diameter (9) were coated with 1.4 mg/ml protein A (Sigma; P-6031) for >30 min in solution A containing 10 mM Pipes, 25 mM K-acetate, 4 mM $MgSO_4$, and 1 mM EGTA (pH 7.0). The bead was then mixed with dynein in solution A containing 3 mg/ml BSA and 0.2 M KCl for 10 min. Dynein-coated beads were trapped, and their position was measured by using an optical trapping system (9). The assay solution was solution A, 10 μM–1 mM ATP, 5 mg/ml BSA, and an oxygen scavenger system at 25 ± 1°C. The trap stiffness was 3–45 fN/nm, determined by the amplitude of the Brownian motion of the beads (9). At a trap stiffness of 40–45 fN/nm (Figs. 2 and 3*a*), displacements to determine the step size and velocity were attenuated by a factor of 1.4 at forces of 1–2 pN to 1.1 at 6–7 pN, because of the stiffness of motor-bead linkage (13, 14). The attenuated displacements were consistent with data where no attenuation was performed at low trap stiffness or zero load (Figs. 3 *e* and *f* and 4*b*).

Individual steps in the movements and the step sizes were automatically detected by using computer programming. Each step was recognized when the step size was >4 nm, and the standard error of noise for 2–16 ms was <1.4 nm. The step size was calculated from the difference between the displacements before and after the step.

An *in vitro* motility assay was performed with some modifications (10). Coverslips were coated with the solution containing protein A as described for coating the beads. Dynein (1–30 nM) was introduced onto coverslips.

Quantum Dot Fluorescence Imaging with 1-nm Accuracy. When imaging quantum dots, the CdSe particles (Evi-dots SG-ETC-H20-600) were cross-linked by using 10 mg/ml 1-ethyl-3-(3-dimethylaminopropyle)carbodiimide (EDC, Pierce) and 2 mg/ml protein A. CdSe–protein A particles (180 nM) were mixed with 30 nM dynein for >15 min. Dynein–CdSe complexes were observed under a fluorescence microscope (IX-71; Olympus, Shinjuku-ku, Tokyo) by evanescent illumination (green laser 0.1 mW/μm^2 at a specimen; Big Sky Laser Technologies, Bozeman, MT) through an objective (Olympus ×60 Planapo, 1.45 numerical aperture, oil) (31). Fluorescence images were captured by using a cooled electron multiplier–charge-coupled device (Ixon DV860; Andor Technology, Tokyo) at 2-ms intervals. The centroid of the bead in the images was determined by fitting the images to 2D Gaussian curves (15). The CdSe particles have significant advantages over other fluorophores in that they have a much higher fluorescence intensity and a longer lifetime. To minimize the blinking of the CdSe particles, three to five CdSe particles with an attached carboxyl group were cross-linked with the amino group of protein A by EDC. Less than 10% of these complexes interacted with the microtubules, indicating that each complex binds only single dynein molecules. The experiments were performed at 16°C.

We thank Jan M. West and Sharyn A. Endow for critically reading this manuscript and Ken'ya Furuta for valuable discussions. This work was supported by Grants-in-Aid for Scientific Research in Priority Areas from the Japan Ministry of Education, Culture, Sports, Science, and Technology (to H.H.); Core Research for Evolutional Science and Technology of Japan Science and Technology Corporation; and Special Coordination Funds for Promoting Science and Technology of Japan Ministry of Education, Culture, Sports, Science, and Technology (to Y.Y.T. and H.H.).

1. Vale, R. D. (2003) *Cell* **112,** 467–480.
2. Hirokawa, N. & Takemura, R. (2004) *Curr. Opin. Neurobiol.* **14,** 564–573.
3. Koonce, M. P. & Samso, M. (2004) *Trends Cell Biol.* **14,** 612–619.
4. Hirakawa, E., Higuchi, H. & Toyoshima, Y. Y. (2000) *Proc. Natl. Acad. Sci. USA* **97,** 2533–2537.
5. Mallik, R., Carter, B. C., Lex, S. A., King, S. J. & Gross, S. P. (2004) *Nature* **427,** 649–652.
6. Paschal, B. M., Shpetner, H. S. & Vallee, R. B. (1987) *J. Cell Biol.* **105,** 1273–1282.
7. Presley, J. F., Cole, N. B., Schroer, T. A., Hirschberg, K., Zaal, K. J. & Lippincott-Schwartz, J. (1997) *Nature* **389,** 81–85.
8. King, S. J. & Schroer, T. A. (2000) *Nat. Cell Biol.* **2,** 20–24.
9. Nishiyama, M., Higuchi, H. & Yanagida, T. (2002) *Nat. Cell Biol.* **4,** 790–797.
10. Toba, S. & Toyoshima, Y. Y. (2004) *Cell Motil. Cytoskeleton* **58,** 281–289.
11. Bingham, J. B., King, S. J. & Schroer, T. A. (1998) *Methods Enzymol.* **298,** 171–184.
12. Nishiura, M., Kon, T., Shiroguchi, K., Ohkura, R., Shima, T., Toyoshima, Y. Y. & Sutoh, K. (2004) *J. Biol. Chem.* **279,** 22799–22802.
13. Svoboda, K. & Block, S. M. (1994) *Cell* **77,** 773–784.
14. Kojima, H., Muto, E., Higuchi, H. & Yanagida, T. (1997) *Biophys. J.* **73,** 2012–2022.
15. Yildiz, A., Forkey, J. N., McKinney, S. A., Ha, T., Goldman, Y. E. & Selvin, P. R. (2003) *Science* **300,** 2061–2065.
16. Warshaw, D. M., Kennedy, G. G., Work, S. S., Krementsova, E. B., Beck, S. & Trybus, K. M. (2005) *Biophys. J.* **88,** L30–L32.

17. Shingyoji, C., Higuchi, H., Yoshimura, M., Katayama, E. & Yanagida, T. (1998) *Nature* **393,** 711–714.
18. Kural, C., Kim, H., Syed, S., Goshima, G., Gelfand, V. I. & Selvin, P. R. (2005) *Science* **308,** 1469–1472.
19. Kon, T., Nishiura, M., Ohkura, R., Toyoshima, Y. Y. & Sutoh, K. (2004) *Biochemistry* **43,** 11266–11274.
20. Carter, N. J. & Cross, R. A. (2005) *Nature* **435,** 308–312.
21. Kaseda, K., Higuchi, H. & Hirose, K. (2003) *Nat. Cell Biol.* **5,** 1079–1082.
22. Asbury, C. L., Fehr, A. N. & Block, S. M. (2003) *Science* **302,** 2130–2134.
23. Yildiz, A., Tomishige, M., Vale, R. D. & Selvin, P. R. (2004) *Science* **303,** 676–678.
24. Hua, W., Chung., J. & Gelles, J. (2002) *Science* **295,** 844–848.
25. Amos, L. A. (1989) *J. Cell Sci.* **93,** 19–28.
26. Goodenough, U. W. & Heuser, J. E. (1982) *J. Cell Biol.* **95,** 798–815.
27. Lupetti, P., Lanzavecchia, S., Mercati, D., Cantele, F., Dallai, R. & Mencarelli, C. (2005) *Cell Motil. Cytoskeleton* **62,** 69–83.
28. Burgess, S. A., Walker, M. L., Sakakibara, H., Knight, P. J. & Oiwa, K. (2003) *Nature* **421,** 715–718.
29. Kon, T., Mogami, T., Ohkura, R., Nishiura, M. & Sutoh, K. (2005) *Nat. Struct. Mol. Biol.* **12,** 513–519.
30. Okada, Y., Higuchi, H. & Hirokawa, N. (2003) *Nature* **424,** 574–577.
31. Tokunaga, M., Kitamura, K., Saito, K., Iwane, A. H. & Yanagida, T. (1997) *Biochem. Biophys. Res. Commun.* **235,** 47–53.

Journal of
Nanoscience and Nanotechnology
Vol. 6, 3503–3506, 2006

X-Ray Absorption of Gold Nanoparticles with Thin Silica Shell

Yeon-Su Park[1,*], Luis M. Liz-Marzán[2], Atsuo Kasuya[1,*], Yoshio Kobayashi[3], Daisuke Nagao[3], Mikio Konno[3], Sergiy Mamykin[1], Andriy Dmytruk[1], Motohiro Takeda[4], and Noriaki Ohuchi[4]

[1] *Center for Interdisciplinary Research, Tohoku University, Sendai 9808578, Japan*
[2] *Departamento de Química Física, Universidade de Vigo, Vigo 36310, Spain*
[3] *Department of Chemical Engineering, Tohoku University, 9808579, Japan*
[4] *Division of Surgical Oncology, Graduate School of Medicine, Tohoku University, Sendai 9808574, Japan*

Silica-coated gold (Au) nanoparticles were prepared and their morphological and X-ray absorption properties were investigated. These core–shell type nanoparticles are very stable in aqueous media and may be suitable for an X-ray contrast agent in biological systems. Transmission electron micrographs confirmed well-separated and relatively homogeneous morphology of the nanoparticles in highly concentrated colloids. Peak position for Au plasmon resonance was red-shifted with increasing shell thickness. X-ray absorption by the colloids of silica-coated Au nanoparticles was stronger than that by those of silica-coated AgI nanoparticles, a recently investigated X-ray contrast agent, at similar experimental conditions.

Keywords: Gold, Silica, Nanoparticles, Core–Shell, X-Ray Absorption, Contrast Agent.

1. INTRODUCTION

Metal nanoparticles are of great interest in both fundamental sciences and practical applications because of their unique size-dependent optical and catalytic properties.[1–5] Especially gold nanoparticles (Au NPs) have attracted huge interest in the research related to biotechnology due to their nontoxic nature, tunable optical properties, and feasibility for surface modification.[6–11]

A typical preparation of colloidal Au NPs with good dispersion involves the reduction of Au^{3+} ions to metallic Au^0 in aqueous media containing citrates, producing the colloids of Au NPs stabilized with citrates.[1–3] The resulting colloids, however, contain low concentration of Au NPs and often require further enrichment process for practical application. Enrichment of colloids, while preserving the shapes and properties of Au NPs, can be achieved by extra surface modification process.[11,12] A widely adapted technique is the surface modification by surface active molecules or macromolecules, which act as a physical barrier against other particles.[12–14] Silica is chemically inert, biocompatible, and highly flexible in surface modification,[5,15] so the formation of silica shell on Au NPs can be a useful way for the stabilization of the nanoparticles. The silica shell enhances colloidal stability in water and permits to control distance between the cores of Au NPs.[12–14] These allow for the preparation of the highly concentrated colloids of Au NPs with silica shell (Au/SiO_2 NPs) for biological applications.

Various microscopic and optical spectroscopic techniques have been utilized to investigate the morphological and optical properties of Au/SiO_2 NPs and their assemblies.[11,12,16–20] X-ray diffraction[19] and photoelectron spectroscopies[20] have been also adapted for studying Au/SiO_2 NPs. However, there have been limited documentations on the use of X-ray absorption techniques for investigating the materials composed of Au NPs and SiO_2.[21,22]

Au has large X-ray absorption coefficient, so it can be an alternative material for an X-ray contrast agent. Currently iodine-containing compounds are used as X-ray contrast agents in computed tomography (CT) scan. They, however, suffer from toxicity by iodine. Au/SiO_2 NPs are nontoxic, very stable in aqueous media, even in their highly concentrated state, and may be suitable for an X-ray contrast agent in biological systems.

In the present work, Au/SiO_2 NPs were prepared and characterized by transmission electron microscopy (TEM), ultraviolet-visible spectroscopy (UV-vis), and X-ray absorption spectroscopy (XAS). To investigate the possibility of the highly concentrated colloids of Au/SiO_2 NPs for an X-ray contrast agent, their relative X-ray transmittances were obtained and compared to those for recently investigated and commercially available contrast agents.

*Authors to whom correspondence should be addressed.

2. EXPERIMENTAL DETAILS

2.1. Chemicals

Hydrogen tetrachloroaurate (III) tetrahydrate ($HAuCl_4 \cdot 4H_2O$), trisodium citrate dehydrate (Na_3-Cit), tetraethyl orthosilicate (TEOS), isopropanol, and ethanol were purchased from Waco Pure Chemicals. 3-Aminopropyl trimethoxysilane (APS) was supplied by Alfa-Aesar. Sodium silicate solution (ca. 27% SiO_2) and DOWEX® 50WX4-400 ion-exchange resin were acquired from Sigma-Aldrich. All chemicals were used as received. Milli-Q water (>18.2 MΩ cm) was used to prepare all solutions.

2.2. Preparation of Materials

Colloids of Au NPs (ca. 18 nm diameter) were prepared by adding preheated 0.17 mM Na_3-Cit solution to boiling 0.50 mM $HAuCl_4 \cdot 4H_2O$ solution under stirring.[20,23] Initial formation of thin silica shell (ca. 4 nm thickness) was made by adding APS (0.25 ml of 1 mM aqueous solution per 100 ml of the colloid) and sodium silicate solution (4 ml of 0.54 wt.% aqueous solution per 100 ml of the colloid) at pH ≅ 10.5 – 11 (adjusted with DOWEX® 50WX4-400 ion-exchange resin) to the colloids of Au NPs, followed by standing the resulting solution (pH ≅ 8.5) for three days.[5,16,20] The well-known Stöber method was adapted for further silica coating on the already-formed thin silica shell.[16,24] Shell thickness was controlled by the amount of TEOS used: 1.80, 5.80, 12.80, and 23.80 μL of TEOS per 10 ml of the colloid of Au NPs prepared from 0.50 mM [Au^{3+}] (27.7 pmol of the Au NPs in the colloid). The resulting colloids of Au/SiO_2 NPs were washed by the combination of centrifugation, supernatant removal, and redispersion in water. Concentrated colloids were prepared by repeating the above-mentioned washing process, while gradually decreasing the amount of water for redispersion each washing cycle. For TEM and UV-vis measurements, the washed and concentrated colloids were diluted with water to the concentration corresponding to 0.5 mM [Au^{3+}] at the time of the Au NP preparation. For convenience, the concentration of metal ions, converted to the value at the time of metal NP preparation, was used to represent the concentration of metal NPs in colloids.

2.3. Characterization

TEM was carried out with a JEOL JEM-2000 microscope. UV-vis was performed with a Hitach U-2000 spectrophotometer. XAS was done with a Rigaku MSXHF[22] spectrophotometer at 20 KeV.

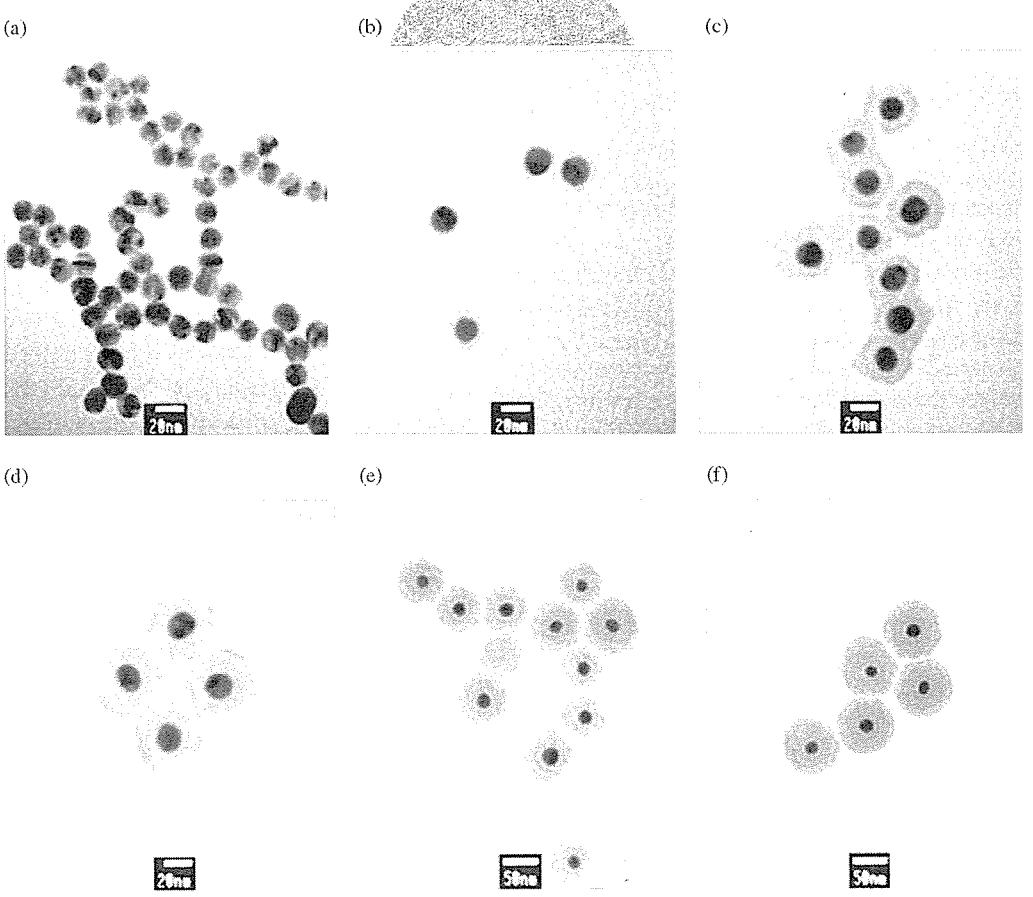

Fig. 1. TEM images of citrate-stabilized (a) and silica-coated (b–f) Au NPs. Silica shells were formed in basic silicate solution (b) and by modified Stöber method at the V_{TEOS}/n_{AuNP} of 0.065 (c), 0.21, (d), 0.46 (e), 0.86 (f) μL/pmol.

3. RESULTS AND DISCUSSION

The citrate-induced reduction of Au^{3+} produced spherical Au NPs with ca. 18 nm diameter. (Fig. 1a) The silica coating processes resulted in relatively homogeneous gold-silica core–shell structures, as shown on TEM images in Figures 1b–f. Silica coating in silicate solution formed spherical silica shell of ca. 4 nm thickness on Au NPs. (Fig. 1b) By shielding van der Waals interaction between Au NPs, the thin silica shell increased stability of the nanoparticles against coagulation in ethanol, a low polarity solvent used for extensive growth of silica shells.[16] As shown on TEM images in Figures 1c–f, further silica coating by the Stöber method resulted in the nanoparticles with thicker silica shells. At the V_{TEOS}/n_{AuNP} of 0.065, 0.21, 0.46, and 0.86 μL/pmol, shell thickness is ca. 13, 16, 24, and 30 nm, respectively. Observation of relatively well-separated spherical nanopartilces after enrichment processes suggests that the silica shells of 4 nm thickness or more effectively shield van der Waals interaction between Au NPs enough to prevent the nanoparticles from flocculation. Sometimes gold-free silica nanoparticles (Fig. 1e) are observed due to the nucleation of remaining silicate ions during transfer of thin silica-coated nanoparticles into ethanol solvent for the preparation of thicker silica shells. Low solubility of TEOS in ethanol causes its fast condensation onto both thin silica-coated Au NPs and gold-free silica nuclei, resulting in thicker silica shells on Au NPs, as well as small amount of gold-free silica nanoparticles.[16]

UV-vis spectra showed red-shift of Au surface plasmon resonance band after silica coating (Fig. 2), due to an increase in the local refractive index of the surrounding medium.[11,16] The change in peak position of the resonance band with silica shell thickness (Fig. 3) is well in accordance with a previous report by Mulvaney and co-workers.[16] They observed a red-shift in the position of the absorption maxima of Au NPs with 15 nm diameter, at silica shell thickness of up to 30 nm, with increasing silica shell thickness and found the same trend in experimental and theoretically calculated peak positions.

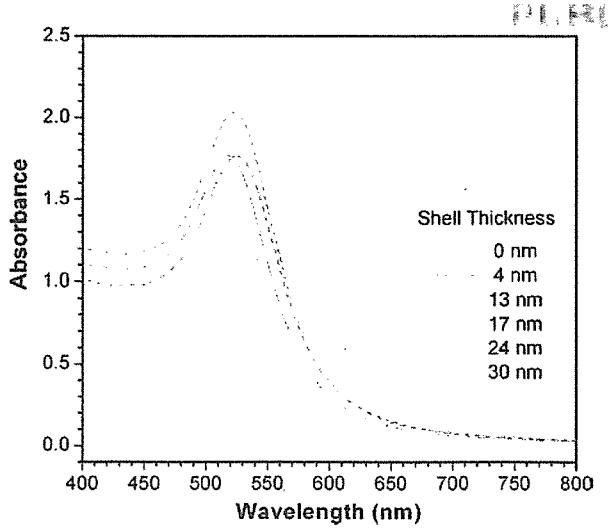

Fig. 2. UV-visible spectra of colloids of citrate-stabilized and silica-coated Au NPs. Concentration of Au, in terms of $[Au^{3+}]$ at the time of the Au NP preparation, was 0.50 mM.

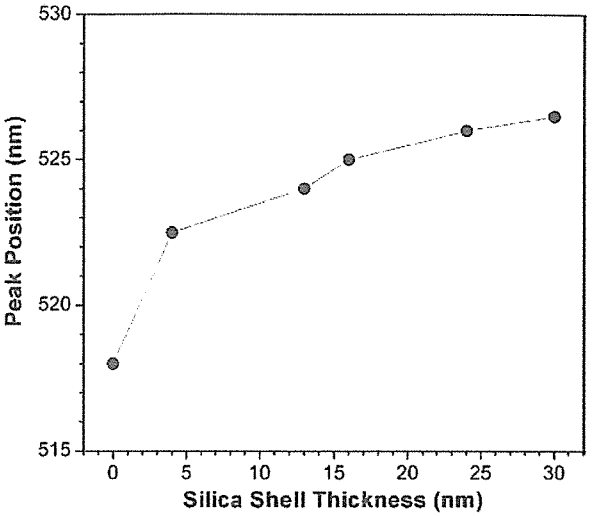

Fig. 3. Influence of silica shell thickness on the peak position of gold plasmon resonance band in Figure 2.

At initial x-ray transmission measurements of 10 times concentrated colloids of Au/SiO_2 NPs (corresponding to $[Au^{3+}] = 5$ mM at the Au NP preparation), Au NPs with thinner silica shells showed lower transmission (higher absorption), compared to those with thicker shells. Relative transmittance of a sample, here defined as the ratio of transmission intensity of a sample to that of water (I_{sample}/I_{water}) were 0.85–0.86 for 4 and 13 nm thick shells and 0.89–1.00 for 16–30 nm thick shells. To obtain lower relative transmittance, colloids of Au NPs with 4 and 13 nm thick shells were further concentrated so that their final concentration reached to 50 mM, in terms of $[Au^{3+}]$ at the Au NP preparation. Their X-ray transmission spectra were obtained and variation in their relative transmittances with time is presented in Figure 4. Relative transmittances are ca. 0.53 and 0.74 for the Au NPs with 4 and 13 nm thick shells, respectively. These values are better than or at least comparable to those obtained by Misawa with the colloids of AgI (24 nm diameter) NPs with 15 nm thick silica shells (AgI/SiO_2 NPs),[25] a recently investigated alternative X-ray contrast agent. In his X-ray absorption studies of colloids of AgI/SiO_2 NPs, relative transmittances of ca. 0.7 and 0.6 were reported at 20 KeV when concentrations of Ag, in terms of $[Ag^+]$ at the Ag NP preparation, were 100 and 200 mM, respectively. Lower or similar relative transmittance of the colloids of Au/SiO_2 NPs at 2–4 times lower metallic concentration, compared to those of AgI/SiO_2 NPs, is mainly due to the difference in X-ray absorption coefficients of two metals: Au has ca. 7 time higher coefficient than Ag at 20 KeV.

In the same studies, a series of successful CT imaging were achieved when concentration of Ag, in terms of $[Ag^+]$ at the Ag NP preparation, was equal to or higher

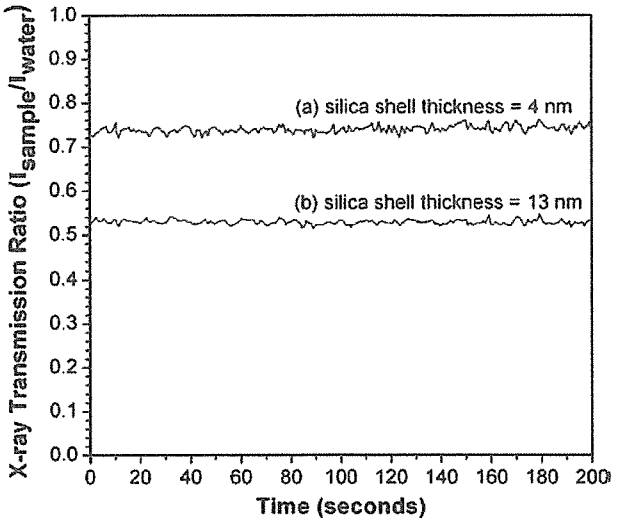

Fig. 4. Variation in relative X-ray transmittance of colloids of Au/SiO_2 NPs with time. Silica shell thickness = 4 (a) and 13 (b) nm. Diameter of Au NPs = 18 nm. Concentration of Au, in terms of $[Au^{3+}]$ at the time of the Au NP preparation, was 50 mM. $V = 2$ KeV, $I = 10$ mA.

than 500 mM. Relative transmittance of the samples used for CT imaging was ca. 0.44. A commercial CT agent (Iopamiron® 300, Japan Schering Co., Ltd.) showed relative transmittance of ca. 0.28 at 20 KeV. These imply that more concentrated colloids of Au/SiO_2 NPs are required to achieve successful CT imaging. Considering higher relative transmittance for Au/SiO_2 NPs at lower metallic concentration, compared to that for AgI/SiO_2 NPs, it will be possible to prepare a practical Au NPs-based X-ray contrast agent. In a practical point of view, because of nontoxic nature of Au, colloidal system of Au/SiO_2 NPs seems to be more attractive than that of AgI/SiO_2 NPs for an X-ray contrast agent.

4. CONCLUSION

Very stable, concentrated colloids of Au NPs were prepared by the formation of silica shells on the surfaces of the NPs, followed by enrichment. By effectively shielding van der Waals interaction between Au NPs, silica shells can minimize coagulation of nanoparticles during washing and enrichment processes. Enrichment process gives little effect on the morphology of Au/SiO_2 NPs and UV-vis absorption characteristics of their colloids. Au/SiO_2 NPs were well-separated each other and showed relatively homogeneous spherical morphology after enrichment. Colloids of Au/SiO_2 NPs showed sharp Au surface plasmon bands and their peak position was red-shifted with increasing shell thickness up to 30 nm. Concentrated colloids of Au/SiO_2 NPs strongly absorb X-ray radiation. The degree of X-ray absorption by colloids of Au NPs with thin (up to 13 nm) silica shells were higher than or at least comparable to that by colloids of AgI/SiO_2 NPs, a recently investigated X-ray contrast agent, at similar experimental conditions. Considering previous successful CT imaging using colloids of AgI/SiO_2 NPs, nontoxic nature of Au, and stronger X-ray absorption by colloids of Au/SiO_2 NPs than by those of AgI/SiO_2 NPs, concentrated colloids of Au/SiO_2 NPs can be a promising candidate for an X-ray contrast agent. More enrichment process and clinical tests are required for their practical application.

Acknowledgments: This work was partially supported by Grant-in-Aid from the Ministry of Education, Science, Sports and Culture, Japan. Authors would like to thank to Mr. K. Toki for help during X-ray absorption measurements.

References and Notes

1. G. Frens, *Nat. Phys. Sci.* 241, 20 (1973).
2. D. G. Duff and A. Baiker, *Langmuir* 9, 2301 (1993).
3. K. C. Graber, K. J. Allison, B. E. Baker, R. M. Bright, K. R. Brown, R. G. Freeman, A. P. Fox, C. D. Keating, M. D. Musick, and M. J. Natan, *Langmuir* 12, 2353 (1996).
4. Y. Kobaysshi, M. Horie, M. Konno, B. Rodríguez-González, and L. M. Liz-Marzán, *J. Phys. Chem. B* 107, 7420 (2003).
5. B. Rodríguez-González, A. Sánchez-Iglesias, M. Giersig, and L. M. Liz-Marzán, *Faraday Discuss* 125, 133 (2004).
6. C. M. Niemyer, W. Bürger, and Jörg Peplies, *Angew. Chem. Int. Ed.* 37, 2265 (1998).
7. T. A. Taton, C. A. Mirkin, and R. L. Letsinger, *Science* 289, 1757 (2000).
8. S.-J. Park, T. A. Taton, and C. A. Mirkin, *Science* 295, 1503 (2002).
9. Y. C. Cao, R. Jin, and C. A. Mirkin, *Science* 297, 1536 (2002).
10. S. R. N. Pena, S. Raina, G. P. Goodrich, N. V. Fedoroff, and C. D. Keating, *J. Am. Chem. Soc.* 124, 7314 (2002).
11. S. Liu and M. Han, *Adv. Funct. Mater.* 15, 961 (2005).
12. E. Mine, A. Yamada, Y. Kobayashi, M. Konno, and L. M. Liz-Marzán, *J. Colloid Interf. Sci.* 264, 385 (2003).
13. C. Chen, T. Takezako, K. Yamamoto, T. Serizawa, and M. Akashi, *Colloids Surf. A* 169, 107 (2000).
14. Y. Kobayashi, K. Misawa, M. Takeda, M. Kobayashi, M. Satake, Y. Kawazoe, N. Ohuchi, A. Kasuya, and M. Konno, *Colloids Surf. A* 251, 197 (2004).
15. T. Schiestel, H. Brunner, and G. E. M. Tovar, *J. Nanosci. Nanotechnol.* 4, 504 (2004).
16. L. M. Liz-Marzán, M. Giersig, and P. Mulvaney, *Langmuir* 12, 4329 (1996).
17. F. Caruso, M. Spasova, V. Salgueiriòo-Maceria, and L. M. Liz-Marzán, *Adv. Mater.* 13, 1090 (2001).
18. F. García-Santamaría, V. Salgueiriòo-Maceria, C. López, and L. M. Liz-Marzán, *Langmuir* 18, 4519 (2002).
19. Y. Yang, M. Hori, T. Hayakawa, and M. Nogami, *Surface Science* 579, 215 (2005).
20. I. Tunc, S. Suzer, M. A. Correa-Duarte, and L. M. Liz-Marzán, *J. Phys. Chem. B* 109, 7597 (2005).
21. Z. Kónya, V. F. Puntes, I. Kiricsi, J. Zhu, J. W. Ager, III, M. K. Ko, H. Frei, P. Alvisatos, and G. Somorjai, *Chem. Mater.* 15, 1242 (2003).
22. D. B. Akolekar, G. Foran, and S. K. Bhargava, *J. Synchrotron Rad.* 11, 284 (2004).
23. I. Pastoriza-Santos, D. Gomez, J. Pérez-Juste, L. M. Liz-Marzán, and P. Mulvaney, *Phys. Chem. Chem. Phys.* 6, 5056 (2004).
24. W. Stöber, A. Fink, and E. Bohn, *J. Colloid Interf. Sci.* 26, 62 (1968).
25. Kiyoto Misawa, M. S. Thesis, Tohoku University, Sendai, Japan (2004).

Received: 8 November 2005. Revised/Accepted: 5 January 2006.

GENERATION OF NANOSIZED SILVER-IODIDE BEADS FOR MEDICAL APPLICATION

YUU SAKURAI [1], MOTOHIRO TAKEDA [2], YOSHIO KOBAYASHI [3], NORIAKI OHUCHI [1]

1) Department of Surgical Oncology, Graduate School of Medicine, Tohoku University, Seiryo-machi 1-1, Aoba-ku, Sendai 980-8574, Japan

2) Department of Bioengineering and Robotics, Graduate School of Engineering, Tohoku University, Aoba 6-6-01, Aoba-ku, Sendai 980-8579 Japan

3) Department of Chemical Engineering, Graduate School of Engineering, Tohoku University, Aoba, Aramaki, Aoba-ku, Sendai 980-8579 Japan

We generated new nanosized silver-iodide beads (AgI) with silica coating for a X-ray contrast medium. Silica-coating was performed to prevent acute and fatal reactions. We also tried to apply AgI for sentinel lymph node biopsy (SNB). SNB can significantly reduce the damage caused by axillary dissection. Radioactive isotopes (RI) is available only for a few institutions and precision of pigment method depends on each doctors' skill. In this study we examined SNB with X ray as a new method to make up for the weak points of traditional approaches. We assessed its temporal distribution with X-CT after subcutaneous and intravenous AgI injection to a rabbit. The contrast-enhancement of a blood vessel, lymph nodes, liver and spleen was observed. Compared with existing contrast media, AgI showed delayed washing out. We can carry out SNB with AgI beads in most institutions which have X-ray equipment and can detect sentinel lymph node more precisely. In addition, AgI nanoparticles may prevent allergic reactions by silica coating, and are expected to be employed in clinical fields by further examination in the future.

Keywords: Nanotechnology, Silver iodide, Sentinel node biopsy, X-ray.

1. Introduction

Now there are various contrast media for X-ray photography. They are useful for angiography or urinary tract contrasting. Several contrast media for computed tomography are currently in use; the two most common are ionic and non-ionic contrast medium (Fig. 1). However emergence of non-ionic contrast media reduced the number of side effects, they still remain an allergic reaction (Table 1). For many years, a lot of studies have been done to overcome these

problems. In this study, we evaluate the possibility of the novel nanosized silver-iodide beads (AgI) with silica coating as a new contrast medium.

The number of breast cancer patients with early-stage is increasing by recent induction of mammography. The role of Sentinel Lymph Node Biopsy (SNB) is getting important, as diagnoses of the presence of axillary lymph node metastasis is a most important prognostic factor of the breast cancer patient. Therefore we need a precise lymph node dissection. We may reduce the damage of axillary lymph node dissection, if SNB is performed for a patient. Now Radioactive Isotopes (RI) or pigments are used commonly. But both of them have problems (Table 2). As for RI method it is impossible to use if there is no radioactive isotope license for the institution. As for the dye method, it is difficult to detect the LNs from outside the skin especially for extraordinary case. In this study we examined SNB with X-ray as a new method to make up for a weak point of traditional approaches.

Fig. 1. Water solubility of ionic (A) and non-ionic (B) contrast media.

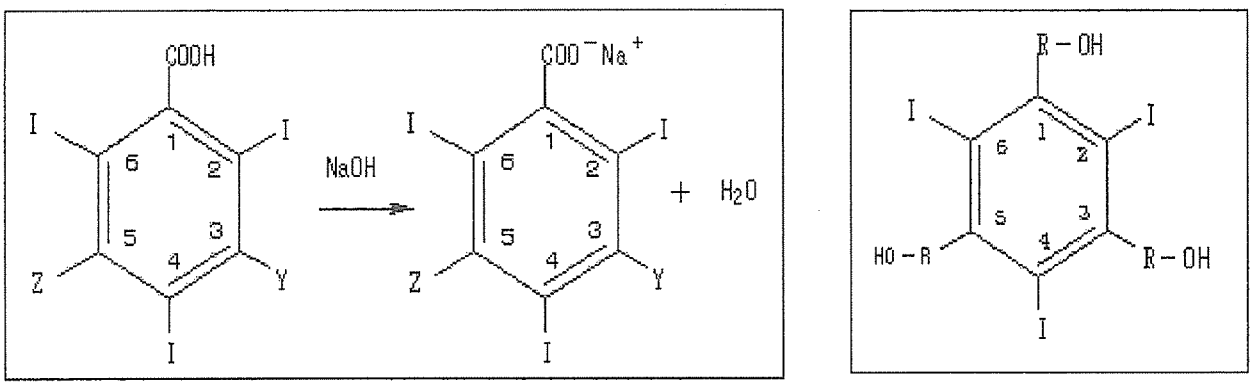

A; Neutralized by NaOH

B; Hydrogen band

Table 1. Side effects of the contrast media.

	Ionic	Non-ionic
Mild symptoms (Pleuritis, nausea, asthma, etc.)	12.66%	3.13%
Severe symptoms (Shock, edema of larynx, etc.)	0.22%	0.04%

2. Methods

We used the AgI ultra-fine particles with silica coated. Silica-coating was performed to prevent acute and fatal reactions. We injected several kinds of different size (40-200nm) of AgI beads into a rabbit (each foot and intravenous injection), and we took a X-CT to evaluate the degree of distribution of AgI beads to a sentinel lymph node, liver, spleen, and kidney.

Table 2. Merit and demerit of the traditional methods.

	Pigment method	**RI method**
Merit	simple	preoperative diagnosability
	low cost	good sensitivity
	less damage	detectable of anomaly
Demerit	technical	facilities
	non-preoperative diagnosability	high cost
		nuclear contamination

3. Results and Discussion

The contrast-enhancement of a blood vessel, lymph nodes, liver and spleen was observed. Compared with existing contrast media, AgI beads showed delayed washing out.

We had already done the experiments using a rat about the nano sized silver iodide beads. And the result showed that AgI beads can be detected and localized by X-ray inside the rat. This time we used different size of beads, and checked its characteristics with a time change. Our latest result of the experiment with fluorescence clarified that the optimal size for short time lymphography was shown to be 40nm. If there is X-ray equipment, we can carry out the identification of a sentinel lymph node by this comparatively simple and convenient method for most institutions. In addition, combining a dye and RI method will make it possible to accomplish more precise LNs dissection with smaller skin incision. We can also use it more safely for many patients to prevent an allergy by the silica coating. Finally in the near future, useful methods and applications are expected in a clinical seat by repeating further examination.

Acknowledgments

The authors acknowledge to the support of 21st Century Center of Excellence (COE) Program "Future Medical Engineering based on Bio-nanotechnology", Japan Society for the Promotion of Science. This study was supported in part by the grant-in-Aid for Research Projects, Promotion of Advanced Medical Technology (H14-Nano-010, and H18-Nano-General-001), from the Ministry of Health, Labor and Welfare of Japan.

References

[1] Kobayashi Y, Misawa K, Takeda M, Kobayashi M, Satake M, Kawazoe Y, Ohuchi N, Kasuya A, and Konno M. Silica-coating of AgI semiconductor nanoparticles. *Colloids and Surfaces A: Physicochem Eng Aspects* **251**, 197–201, 2004.

[2] Kobayashi Y, Misawa K, Kobayashi M, Takeda M, Konno M, Satake M, Kawazoe Y, Ohuchi N, and Kasuya A. Silica-coating of fluorescent polystyrene microspheres by a seeded polymerization technique and their photo-bleaching property. *Colloids and Surfaces A: Physicochem Eng Aspects* **242**, 47–52, 2004.

[3] Nakajima M, Takeda M, Kobayashi M, Suzuki S, and Ohuchi N. Nano-sized fluorescent particles as new tracers for sentinel node detection: experimental model for decision of appopriate size and wavelength. *Cancer Sci* **96**, 353-356, 2005.

[4] Kobayashi Y, Misawa K, Kobayashi M, Takeda M, Konno M, Satake M, Kawazoe Y, Ohuchi N, and Kasuya A. Silica-coating of fluorescent polystyrene microspheres by a modified Stober method and their stability against photo-bleaching. *e-Polymers* **052**, 1-8, 2005.

DEVELOPMENT OF SILICA COATED SILVER IODIDE NANO-PARTICLES IN DIFFERENT SIZES FOR NOVEL X-RAY CONTRAST MEDIA

LIMAN CONG [1)†], YOSHIO KOBAYASHI [2)], MOTOHIRO TAKEDA [3)], NORIAKI OHUCHI [1)]

1) Department of Surgical Oncology, Graduate School of Medicine, Tohoku University, 1-1 Seiryo-machi , Aoba-ku, Sendai 980-8574, Japan

2) Department of Chemical Engineering, Graduate School of Engineering, Tohoku University, 07 Aoba, Aramaki-aza, Aoba-ku, Sendai 980-8579, Japan

3) Department of Bioengineering and Robotics Graduate School of Engineering, Tohoku University,6-6-01 Aoba, Aoba-ku, Sendai 980-8579, Japan

The breast cancer incidence and the mortality are increasing. Accurate diagnosis of the malignancy is the most important issue. In this study we produced silver iodide (AgI) nano-particles as a useful and safe X-ray contrast media. We employed Stöber method using TEOS to produce silica-coated AgI nano-particles. We produced two types of nano-particles of different average sizes. Our novel contrast media can be used not only for vascular enhancement but also sentinel lymph node biopsy by modifying the size of the particles. We are now studying the dynamics and the excretion pathway of the silica-coated AgI nano-particles in rats by TEM to establish safety.

Keywords: Nanotechnology, Silver iodide, X-ray.

1. Introduction

Nanotechnology for medical diagnosis is rapidly developing along with the innovation of detection techniques. Functional nano-particles and nanometer detection techniques are the most expected issues for the evolution of medicine.

The breast cancer incidence and the mortality are increasing and the early and accurate diagnoses are the most important issues. The incidence of the breast cancer occupies the majority of women in Japan. It is urgent to establish "made-to-order medicine" to perform suitable therapy for each patient of different stages. The "order to made medicine" is based on accurate diagnosis and proper

† Liman Cong has been a Tohoku University 21COE Research Assistant from 2005 to 2006.

treatment. Accurate estimation of the extent of malignancy is the most important issue for "made-to-order treatment".

Enhanced X-CT is essential for staging of malignancies with their vascularity. It can clearly visualize the existence and extent of malignancy. Existing contrast media made with iodine have a possibility of allergy when it is administered in patients. Although, development of non-ionic contrast media reduced incidence of allergy, total resolve of the allergy is expected, for we cannot administer iodine contrast media to a patient with episodes of iodine allergy.

Sentinel node navigation surgery is emerging as an "made-to-order surgery" for carcinomas in early stages. The sentinel node (SN) is the first lymph node on the lymphatic drainage pathway from the cancerous tumor. In cases where the SN has a metastasis, there is the possibility of another positive node. When the SN is negative for metastasis, we can consider that there will be no other positive node and lymph node dissection (LND) is not necessary except for the SN [1]. This leads to the avoidance of functional or organic complication after LND. There are two major methods for detection of SN using tracer molecules or particles. Dyes and/or radioisotopes have been employed for SN detection in standard method, however each detection method has advantages and disadvantages. The dye method is not available for pre-operational detection of SNs. And there are few hospitals in which radioisotope method is available for some regulations. Thus, a new non-invasive method that makes up for the disadvantages is expected.

In this study, we aimed to develop silica coated silver-iodide nano-particles of uniform size as safe and useful X-ray contrast media those enable vascular enhancement and visualizing SN from outside the body by X-CT, and conducted experiments to establish the method to produce novel nano-sized X-ray contrast media.

2. Materials and Methods

2.1. *Chemicals*

Silver perchlorate ($AgClO_4$) (Kanto Chemical Co. Inc., 99%) and potassium iodide (KI) (Wako Pure Chemicals Ltd., 99.5%) were used as silver precursors. Tetraethoxyorthosilicate (TEOS) (Wako Pure Chemicals Ltd., 95%), 3-mercaptopropyltrimethoxysilane (MPS) (Aldrich, 97%), ethanol (Wako Pure Chemicals Ltd., 99.5%) and Sodium hydroxide solution (NaOH) (Wako Pure Chemicals Ltd.) was used for silica-coating [2].

All chemicals were used as received. Ultra pure deionized water (resistivity higher than 18 MΩ cm) was used in all the preparations.

2.2. *Silica-Coating of AgI*

The Stöber method using TEOS was employed for silica-coating of the AgI nano-particles. We added 2×10^{-3} M of KI, 1×10^{-3} M of $AgClO_4$, and 4.5×10^{-5} M of MPS into ultra pure water, respectively. After 15min we added 99.5% Ethanol, 0.008M of TEOS and 1.1×10^{-3} M of NaOH. Then we incubated the solution at 15℃～16℃ for (or "up to") 12 hours [3] (Fig. 1).

The size of silica coated AgI particles was estimated with a transmission electron microscopy (TEM).

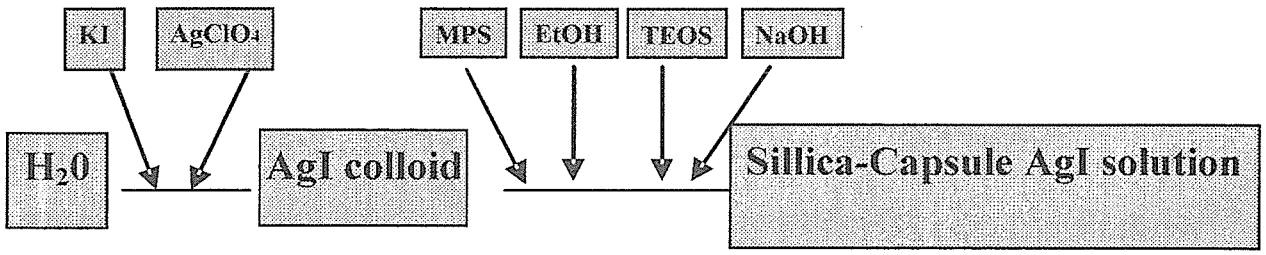

Fig. 1. Pattern chart of making method for AgI nano-particles.

3. Results and Discussion

We could successfully make up two different sizes of silica-coated AgI nano-particles. The average size of silica coated AgI particles was 30nm and 50nm in diameter as shown in Fig. 2.

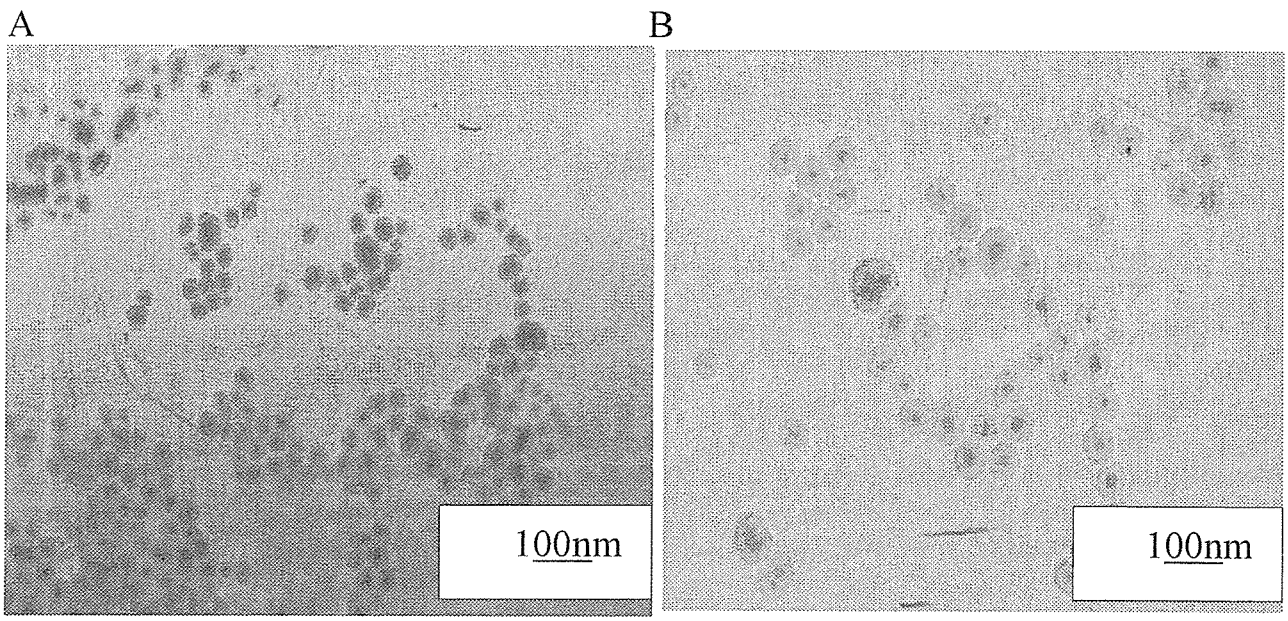

Fig. 2. A: TEM image of silica-coated AgI–SiO2 nanoparticles in size of 30 nm.
B: TEM image of silica-coated AgI–SiO2 nanoparticles in size of 50 nm.

As our colleague noted in another part in this book, we could obtain enhanced images of a rat. We can clearly observe the enhancement in the spleen in Fig. 3 as an example. An inguinal sentinel node could be also detected by subcutaneous injection in feet of rats and rabbits (images not shown).

In this study, we could produce two sizes of AgI nano-particles. The silica coated silver iodide nano-particles have two advantages. The first is that it is physically and chemically stable and they prevent allergy when they are administered to a body. The second is that we can modify their size according to our purposes by changing thickness of silica shell. Smaller size like 30 nm is suitable for vascular enhancement and the size around 40 nm or more is suitable for SN detection [1].

Safety of nano-particles is very important for medical applications. Now we are studying dynamics of AgI nano-particles in the body by TEM and estimating LD_{50} for the next step of the development.

In the near future, our novel X-ray contrast media can be used as both vascular contrast media and sentinel lymph node enhancers, for we can produce different sizes of nano-particles.

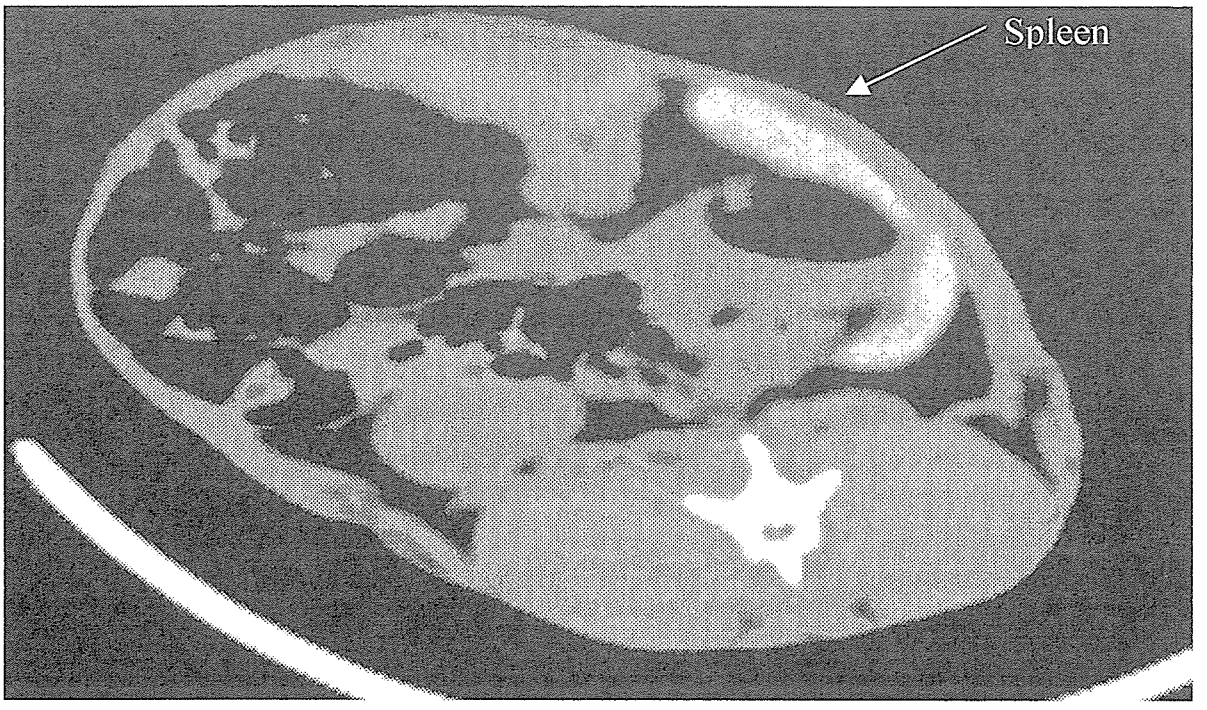

Fig. 3. Enhanced CT image of a rat spleen, 5 minutes after venous injection of AgI nano-particles.

Acknowledgments

We are grateful to the support by Grants-in-aid for Research Project, Promotion of Advanced Medical Technology (H14-Nano-010 and H18-Nano-001), from the Ministry of Health, Labor and Welfare of Japan, and the support by Tohoku University 21st Century Center of Excellence (COE) Program "Future Medical Engineering based on Bio-nanotechnology".

References

[1] Nakajima M, Takeda M, Kobayashi M, Suzuki S, and Ohuchi N. Nano-sized fluorescent particles as new tracers for sentinel node detection: experimental model for decision of appropriate size and wavelength. *Cancer Sci* **96**, 353-357, 2005.

[2] Kobayashi Y, Misawa K, Takeda M, Kobayashi M, Satake M, Kawazoe Y, Ohuchi N, Kasuya A, and Konno M. Silica-coating of AgI semiconductor nanoparticles. *Colloids and Surfaces A: Physicochem Eng Aspects* **242**, 47-52, 2004.

[3] Kobayashi Y, Misawa K, Takeda M, Kobayashi M, Satake M, Kawazoe Y, Ohuchi N, Kasuya A, and Konno M. Slica-coating of AgI semiconductor nanoparticles. *Colloids and Surfaces A: Physiochem Eng Aspects* **251**, 197–201, 2004.